Malaysian Journal of Analytical Sciences, Vol 20 No 4 (2016): xxx - xxx
DOI: http://dx.doi.org/10.17576/mjas-2016-2004-zz

MALAYSIAN JOURNAL OF ANALYTICAL SCIENCES
Published by The Malaysian Analytical Sciences Society
ISSN 1394 - 2506

PREPARATION AND CHARACTERIZATION OF Cu-Fe/TiO_2 PHOTOCATALYST FOR VISIBLE LIGHT DEEP DESULFURIZATION

(Penyediaan dan Pencirian Fotokatalis Cu-Fe/TiO_2 untuk Proses Nyahsulfur Di Bawah Cahaya Tampak)

Hayyiratul Fatimah Mohd Zaid[1], Chong Fai Kait[1]*, Mohamed Ibrahim Abdul Mutalib[2]

[1]*Department of Fundamental & Applied Sciences*
[2]*Department of Chemical Engineering*
Universiti Teknologi PETRONAS, 32610 Seri Iskandar, Perak., Malaysia

**Corresponding author: chongfaikait@petronas.com.my*

Received: 17 August 2015; Accepted: 23 May 2016

Abstract

A photooxidative system for deep desulfurization of model diesel fuel was explored. Nanoparticles of anatase titania (TiO_2) were synthesized via sol-gel hydrothermal method. The TiO_2 was further modified with bimetallic Cu-Fe using wet-impregnation method followed by calcination process in order to extend the activity region of the photocatalyst to visible-light. A series of bimetallic 2.2 wt% Cu-Fe/TiO_2 photocatalysts with different Cu:Fe mass compositions were characterized for their physical, chemical and optical properties using X-ray diffraction (XRD), field emission scanning electron microscopy (FESEM), high resolution transmission electron microscopy (HRTEM), diffuse reflectance UV-visible spectroscopy (DR-UV-Vis), Fourier Transform Infrared Spectroscopy (FTIR) and Brunauer–Emmett–Teller (BET) surface area analysis. The performance of the photocatalysts was evaluated for photooxidation of dibenzothiophene (DBT) as the sulfur species from model oil in the presence of hydrogen peroxide, H_2O_2 under 500 W visible light illumination. The highest sulfur conversion of 82.36 % was observed for photocatalyst with 10:1 Cu:Fe mass composition.

Keywords: photocatalyst, titania, oxidation, desulfurization, visible light, copper-iron

Abstrak

Sistem fotopengoksidaan untuk proses nyahsulfur daripada model minyak diesel dikaji. Nanopartikel titania (TiO_2) dengan fasa anatas disediakan menggunakan kaedah hidrotermal sol-gel. Pengubahsuaian dengan dwilogam Cu-Fe dilakukan terhadap TiO_2 menggunakan kaedah impregnasi basah diikuti dengan proses pengkalsinan untuk melanjutkan aktiviti fotokatalis ke bahagian cahaya tampak. Siri fotokatalis dwilogam 2.2 wt% Cu-Fe/TiO_2 dengan komposisi jisim Cu:Fe yang berlainan dicirikan untuk menentukan sifat-sifat fizikal, kimia and optik menggunakan pembelauan sinar-X (XRD), pemancaran medan mikroskopi imbasan elektron (FESEM), mikroskopi transmisi elecktron beresolusi tinggi (HRTEM), spektroskopi pantulan resapan ultraungu-tampak (DR-UV-Vis), spektroskopi transformasi Fourier inframerah (FTIR) dan analisis luas permukaan Brunauer–Emmett–Teller (BET). Kajian terhadap fotopengoksidaan dibenzothiophene (DBT) sebagai spesis sulfur di dalam model minyak menggunakan fotokatalis tersebut dilakukan dengan kehadiran hidrogen peroksida, H_2O_2 di bawah sinaran cahaya tampak 500 W. Prestasi tertinggi penukaran sulfur yang tercapai adalah 82.36 %, daripada fotokatalis yang mempunyai komposisi jisim untuk Cu:Fe sebanyak 10:1.

Kata kunci: fotokatalis, titania, pengoksidaan, nyahsulfur, cahaya tampak, kuprum-besi

Introduction

Energy production is one of the most pressing issues of the modern world. The main task of modern refinery is to efficiently produce high yields of valuable products. Gasoline, diesel and non-transportation fuel comprises 75 – 80 % of refinery products. Environmental restrictions regarding the quality of transportation fuels produced and the emissions from the refinery itself are currently the most important issues, as well as the most costly to meet. Sulfur species represent one of the most common impurities in crude oil [1]. The distribution of the sulfur species mainly depend on the origin of the petroleum, type and volume of different stream feeding into the diesel pool. Diesel feeds contain a large number of individual sulfur species, such as dibenzothiophene (DBT) and alkyl derivatives [2].

Sulfur species are undesirable in the refining process as they tend to deactivate some catalysts used in the crude oil processing and cause corrosion problems in pipelines, pumping and refining equipment. Naturally occurring residual sulfur species in fuels will lead to the emission of sulfur oxide gases during combustion. These gases react with water in the atmosphere to form sulfates and acid rain which can damage buildings, destroy automotive paint finishes, acidifies soil and ultimately lead to destruction of forest and various other ecosystems. Sulfur emission also causes respiratory problems, heart diseases, asthma and contributes to the formation of atmospheric particulates. Automobiles are also adversely affected by the presence of sulfur species in the fuels, as the sulfur species have a profound effect on the efficacy of catalytic converters [3].

The current industrial method for removal of sulfur species from fuels is known as hydrodesulfurization (HDS), which operates at high temperature and pressure. This makes HDS a very costly option for deep desulfurization. In addition, HDS is not effective in removing refractory heterocyclic sulfur species such as DBT and its derivatives, especially 4,6-dimethyldibenzothiophene (4,6-DMDBT) [4, 5]. Oxidative desulfurization (ODS) [6, 7], extractive desulfurization (EDS) [8, 9], adsorptive desulfurization [10, 11] and biodesulfurization (BDS) [12, 13] are other desulfurization techniques that have the potential to produce ultra clean fuel. In ODS, the sulfur species are oxidized to sulfone by chemical reaction using oxidants such as hydrogen peroxide (H_2O_2), nitric acid, ozone, air and others.

Recently, research has focused on investigating the desulfurization of sulfur species via photocatalysis [14, 15] utilizing radiation energy. Titanium dioxide (TiO_2) based photocatalysis has been widely employed in environmental purification to decompose organic compounds in air and wastewater since this method can be conducted under mild reaction conditions [16]. Moreover, TiO_2 is inert to chemical corrosion, has a strong oxidizing power (with UV light) and is cost effective [17]. The successful application of photocatalysis in deep desulfurization process has been reported previously to remove thiophenes and derivatives of benzothiophene (BT) and DBT, which are the model sulfur species in gasoline [18, 19], light oil [14, 20] and diesel [21]. The results indicated that photodesulfurization has displayed higher activity compared to the conventional HDS in removing refractory DBT derivatives such as 4-methyldibenzothiophene (4-MDBT) and 4,6-DMDBT [14].

As reported by Matsuzawa et al. [22], DBT and 4,6-DMDBT in acetonitrile are photooxidized to 5-oxide (sulfoxide) and 5,5-dioxide (sulfone) using TiO_2. The application of this photochemical oxidation to desulfurization as been realized in some literatures [22, 23] using oil-water and oil-polar solvent two phase systems. The desulfurization of light oil to a sulfur content of less than 0.05 wt% has been achieved successfully. However, ultraviolet (UV) irradiation was found to be essential to oxidize DBTs and the desulfurization hardly progresses at wavelength, $\lambda > 400$ nm. Therefore, there is a need to develop a photocatalyst system that enables the use of renewable energy resources such as sunlight which provides cleaner and more efficient removal of sulfur species from petroleum fuel oils. Incorporation of transition metal onto TiO_2 structure could produce photocatalyst that displays activity in visible light. Iron (Fe) and copper (Cu) have received much attention as metal dopants as these metals are cheap and abundant in supply. A great deal of research has been conducted using Cu or Fe doped TiO_2, but co-doped Cu and Fe onto TiO_2 is rarely reported. Liu et al. [24] and Zhang [25] degraded organic dye pollutants, Reactive Black 5 (RB 5) and Methyl Orange (MO) in wastewater under UV [24] and visible light [25] radiation, respectively. They showed that co-doped Cu and Fe onto TiO_2 displayed significant enhancement in photodegradation of the organic dye pollutants compared to the un-doped TiO_2.

This paper focused on the synthesis and characterization of Cu-Fe/TiO_2 photocatalysts for the photooxidation of sulfur species in model oil under visible light radiation. Further treatment to the model oil is required in order to

remove the oxidized sulfur species and also the residual sulfur species in order to complete the deep desulfurization process. Example of such treatment is extraction using eutectic ionic liquids which was reported in a separate work [26].

Materials and Methods

Materials and reagents

Titanium tetraisopropoxide, TTIP ($Ti(OC_3H_7)_4$) (Merck, 97 %), *n*-heptane (C_7H_{16}) (Fisher, 99 %), anhydrous iron(III) chloride ($FeCl_3$) (Merck, 98 %), copper(II) chloride dihydrate ($CuCl_2.2H_2O$) (Merck, 99 %), dibenzothiophene, DBT ($C_{12}H_8S$) (Merck, 98 %) and dodecane ($C_{12}H_{26}$) (Merck, 98 %) were used without further purification.

Synthesis of TiO_2

Nanoparticle TiO_2 was synthesized using a method modified from that reported by Khan et al. [27]. An amount 27 mL of titanium tetraisopropoxide (TTIP) was added into 100 mL of *n*-heptane as a solvent. The mixture was stirred at 300 rpm for 2 hours. This was followed by drop wise addition of 7.98 mL distilled water to the mixture, giving a molar ratio of 1:5 for TTIP:H_2O. The mixture was left to age for 72 hours at room temperature. The obtained sol was transferred to a 100 mL teflon-lined autoclave vessel and was heated to 240 ^oC for 12 hours. The resulting precipitate was dried in the oven at 70 ^oC for 12 hours. After drying, the raw TiO_2 was calcined in a furnace at 500 ^oC in ambient air for 1 hour. The calcination process was carried out to remove any residual organic substance and also as an activation process to transform the hydroxides into anatase TiO_2.

Preparation of Cu-Fe/TiO_2

A series of 2.2 wt% Cu-Fe/TiO_2 photocatalysts with different Cu:Fe mass composition (10:1, 9:2 and 8:3) was prepared using wet impregnation method. $CuCl_2.2H_2O$ and $FeCl_3$ were used as metal precursors. Predetermined amounts of $CuCl_2.2H_2O$ and $FeCl_3$ salts were dissolved in distilled water with continuous stirring. The required amount of TiO_2 support was added into the metal salt solution. The suspension was stirred for 1 hour before the solvent was evaporated in a water bath at 80 ^oC and further dried in an oven at 120 ^oC for 18 hours. The raw photocatalysts were ground into fine powder and then calcined at 500 ^oC for 1 hour (10 $^oC \cdot min^{-1}$ ramping). The temperature selected was adopted from previous reported method [26]. The denotation of the photocatalysts was: xCuyFe, where 'x' represents the amount of Cu and 'y' represents the amount of Fe in which 'x' + 'y' = 11. For example, 10Cu1Fe refers 2.2 wt% Cu-Fe/TiO_2 photocatalyst with 10:1 Cu:Fe mass composition. Monometallic Cu/TiO_2 and Fe/TiO_2 photocatalysts with 2.2 wt% metal loading, denoted as Cu and Fe, respectively, were also prepared for comparison purposes.

Characterization of photocatalysts

The X-ray diffraction (XRD) patterns of the calcined TiO_2 and also the prepared Cu-Fe/TiO_2 photocatalysts were recorded using Bruker D8 Advance with CuKα radiation (40 kV, 40 mA) at 2θ angles from 2 to 80^o and a scan speed of 4 $^oC \cdot min^{-1}$ to determine the active TiO_2 phase present. Morphology of the photocatalysts were examined using field emission scanning electron microscopy (FESEM, Supra55VP) coupled with energy dispersive X-ray analysis (EDX) and high resolution transmission electron microscopy (HRTEM, Zeiss Libra 200). The light absorption properties of the photocatalysts were recorded using diffuse reflectance UV-visible spectroscopy (DR-UV-Vis) where the Shimadzu Spectrometer 3150 was equipped with an integrated sphere assembly in which $BaSO_4$ was used as the reference material. Tauc Plot, derived from DR-UV-Vis spectrum was employed to determine the band gap energy of the photocatalysts. The BET surface area of the photocatalysts was determined using surface analyzer (Tristar II 3020). Fourier Transform Infrared (FTIR) spectra of the photocatalysts were scanned from 4000 to 450 cm^{-1} at 1.2 cm^{-1} resolution using Perkin Elmer Spectrophotometer. The surface area and pore volume were calculated using the Brunauer-Emmett-Teller (BET) method, and pore size distribution was determined from the desorption branch of the desorption isotherm by the Barrett-Joyner-Halenda (BJH) method.

Photooxidative deep desulfurization process

The photooxidation process involved suspending the photocatalyst in model oil containing 100 ppm dibenzothiophene (DBT) as the model sulfur species in dodecane. Photooxidation was carried out in a glass photoreactor positioned below the light source (500W halogen lamp, λ >400 nm) at a distance 15 cm from the lamp.

The model oil was mixed with 1 $g \cdot L^{-1}$ of photocatalyst. H_2O_2 with a molar ratio of 4:1 (H_2O_2:S) was added and the suspension was stirred in the dark for 30 min to achieve adsorption-desorption equilibrium between DBT in the model oil and the photocatalyst. Subsequently, photooxidation process occurred under visible light illumination. The photooxidation process was monitored by periodic sampling where the photocatalyst was separated from the model oil by filtration prior to analysis using GC-SCD (Agilent 7890A gas chromatograph coupled with Agilent 355 sulfur chemiluminescence detector). The DB-1 J & W 123-1033 (30 m x 320 um x 1 um) column was maintained at 325^oC with helium as carrier gas flowing at 1.1 $mL \cdot min^{-1}$. The auto sampler was in split mode (300 ^oC, 6.16 psi, 50:1 split ratio at 55 $mL \cdot min^{-1}$, split flow 50 $mL \cdot min^{-1}$, septum purge flow 3 $mL \cdot min^{-1}$) and injection volume of 1.0 µL. The detector settings were: burner at 800 ^oC (to ensure complete sulfur combustion), dual plasma controller at 250 – 400 torr, 65 sccm of air flow rate, 40 sccm of H_2 flow rate and 20 – 30 $mL \cdot min^{-1}$ at 3 – 6 psi of ozone flow rate. The efficiency in converting sulfur species to oxidized sulfur species in the model oil was calculated using equation (1):

$$\text{Sulfur conversion } (\%) = \frac{S_i - S_f}{S_i} \, x \, 100 \, \% \quad (1)$$

where, S_i and S_f refer to the initial and final concentrations of sulfur species (DBT) in model oil.

Results and Discussion

X-ray diffraction

The effect of Cu:Fe mass composition on the crystallite phase and crystallinity of the photocatalysts was analyzed. Figure 1 display the XRD patterns of Cu-Fe/TiO_2 with different Cu:Fe mass composition (10:1, 9:2 and 8:3). The photocatalysts were calcined at 500 ^oC for 1 hour prior to analysis. All the samples displayed the typical anatase TiO_2 crystal structure with peaks at 2θ of 25.3°, 38.0°, 48.3°, 54.8°, 55.8° and 62.6° corresponding to (101), (004), (200), (105), (211) and (204) phases, respectively [27, 28]. The preferred orientation corresponding to the phase (101) is observed in all the samples. Both monometallic TiO_2 (Cu and Fe) and bimetallic Cu-Fe/TiO_2 photocatalysts displayed high intensity for the diffraction peak at 2θ = 25.3^o. This indicates larger crystallite size compared to bare TiO_2. There was no indication of the presence of Cu, Fe or Cu-Fe species in all the XRD patterns. This may be due to the presence of highly dispersed Cu and Fe species and also low metal content [29], which are below the detection limit of the equipment [30]. In order for the metal to be detectable by XRD analysis, the concentration of metals should be higher than 5wt% [31]. However, the presence of the incorporated metals can be confirmed from EDX mapping that will be discussed in later section. No peaks attributed to the rutile phase could be detected. This may be due to the calcination temperature, as the transition from anatase to rutile phase normally occurs at temperature above 600 ^oC.

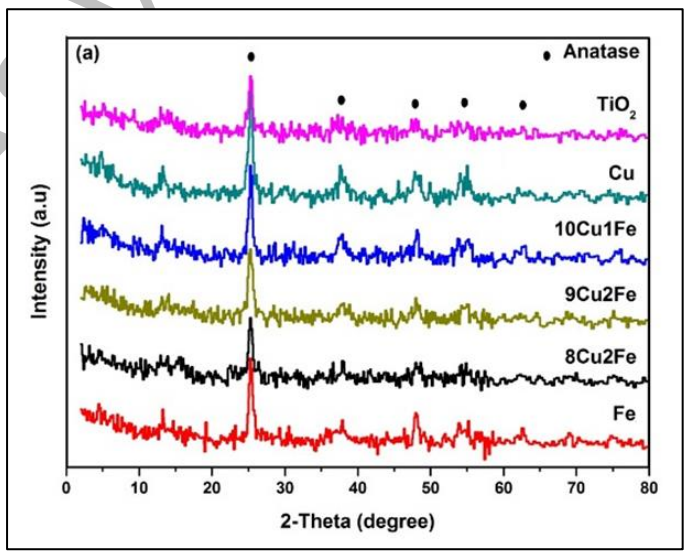

Figure 1. XRD patterns of TiO_2, Cu, 10Cu1Fe, 9Cu2Fe, 8Cu3Fe and Fe

The dominant peak at 25.3° (101) was used to estimate the crystallite size of the photocatalyst using Debye Scherrer's equation [32]. The average crystallite sizes for the photocatalysts are listed in Table 1. The estimated crystallite size for TiO_2 was 11.50 nm. Monometalic Fe showed larger crystallite size compared to monometallic Cu. For the bimetallic photocatalysts, as the composition of Cu decreased, the average crystallite size also showed a decreasing trend. Higher Fe content led to smaller crystallite size in the bimetallic system. Incorporating both Cu and Fe metals decreases the crystallite size compared to single doping. This could be caused by restrained grain growth in the presence of both Cu and Fe, which in turn led to smaller crystallite size at certain mass composition. Similar trend was reported by Kim and Kang [33] where incorporation of both Cu and Ag produced smaller crystallites compared to single doped photocatalyst.

Table 1. Crystallite and particle sizes of photocatalysts from different analysis methods

Sample	Average Crystallite Size (nm)	Particle Size Range (nm)	
	XRD	FESEM	HRTEM
TiO_2	11.50	10.39 – 15.79	10.88 – 16.24
Cu	18.22	17.78 – 19.04	18.03 – 26.11
10Cu1Fe	17.42	17.34 – 17.61	13.51 – 20.67
9Cu2Fe	17.34	17.21 – 17.58	12.92 – 21.01
8Cu3Fe	17.06	16.92 – 17.12	13.04 – 19.17
Fe	19.92	19.84 – 20.11	11.61 – 22.37

Field Emission Scanning Electron Microscopy

FESEM micrographs of photocatalysts at different Cu:Fe mass composition are shown in Figure 2 (a-f). The particles were spherical in shape with slight agglomeration observed for all the photocatalysts. As the Cu:Fe mass composition decreased from 10:1 to 9:2 and 8:3, the average particle size decreased from 17.53, 17.43, and 17.20 nm, respectively. The particles of TiO_2 were small compared to the metal doped photocatalysts with particle size ranging from 10.39 – 15.79 nm (average particle size of 11.39 nm). The average particle size of monometallic Cu and Fe were 18.44 and 20.12 nm, respectively, comparable to the trend observed on the average crystallite sizes from XRD analysis. Detailed particle size distribution as provided in Table 1. No localized metal particles were detected, indicating high metallic dispersion of Cu and Fe on TiO_2. This observation is in agreement with the results obtained from XRD analysis.

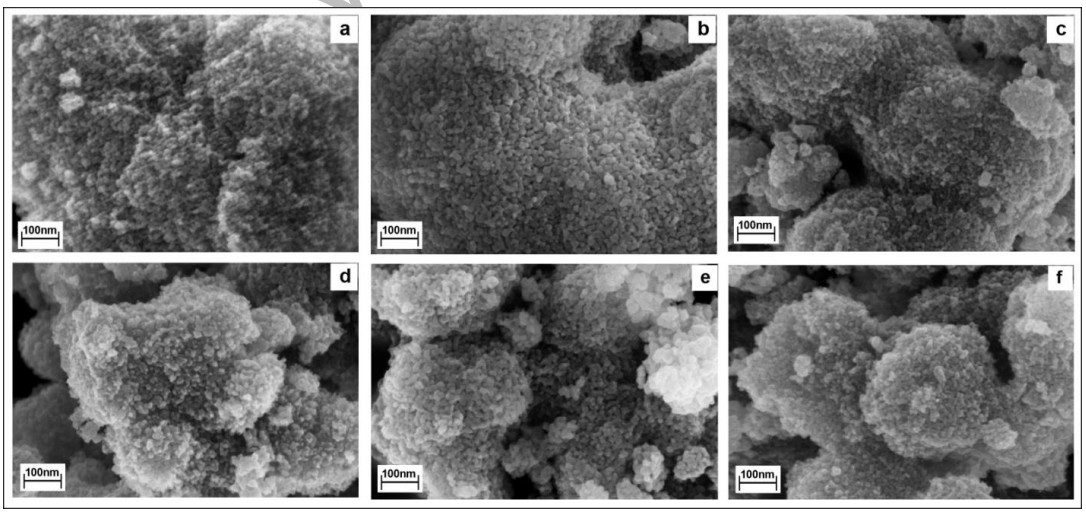

Figure 2. FESEM micrographs of (a) TiO_2, (b) Cu, (c) 10Cu1Fe, (d) 9Cu2Fe, (e) 8Cu3Fe and (f) Fe (100 kX magnification)

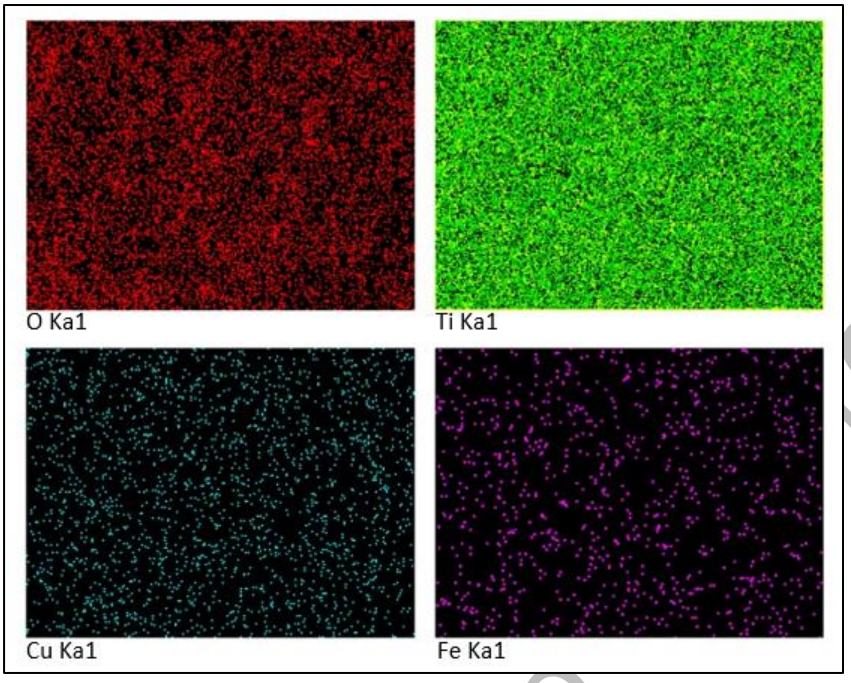

Figure 3. EDX and mapping images of 10Cu1Fe

High Resolution Transmission Electron Microscopy

HRTEM analysis was carried out to determine the detailed morphology of the photocatalyst. Image processing analysis of HRTEM micrographs was used to refine the microstructures for more accurately analyzed single grains and grains boundaries. Figure 4 (a-f) shows the HRTEM micrographs of Cu-Fe/TiO_2 photocatalysts at different Cu:Fe mass compositions. All micrographs showed good crystallite morphology of the particles with mixtures of spherical and polygonal shapes [36]. TiO_2 has the most polygons and as the Fe content increased, the particles became more spherical. The estimated particle sizes of the photocatalysts are tabulated in Table 1. These particle size distribution are in good agreement with the data extracted from FESEM analysis. HRTEM micrographs of the photocatalysts showed agglomeration of particles. This is possible due to high content of surface hydroxyl groups contributing towards the hydrophilic properties [37].

Brunauer-Emmett-Teller

Isotherm plot of 10Cu1Fe is shown in Figure 5. The plot shows Type IV isotherm with hysteresis loop indicating mesoporous structure. The inflection points showed P/Po range of 0.6 – 1.0. The other photocatalysts also displayed similar isotherm. The pore distribution of the photocatalysts was determined by BJH method. Cu-Fe/TiO_2 photocatalysts are mesoporous with an average pore diameter (4V/A) of 13.76, 13.30 and 14.06 nm for 10u1Fe, 9Cu2Fe and 8Cu3Fe, respectively. The BET surface area of the materials for 10u1Fe, 9Cu2Fe and 8Cu3Fe were 49.99, 42.11 and 45.33 m^2/g, respectively, which was comparable.

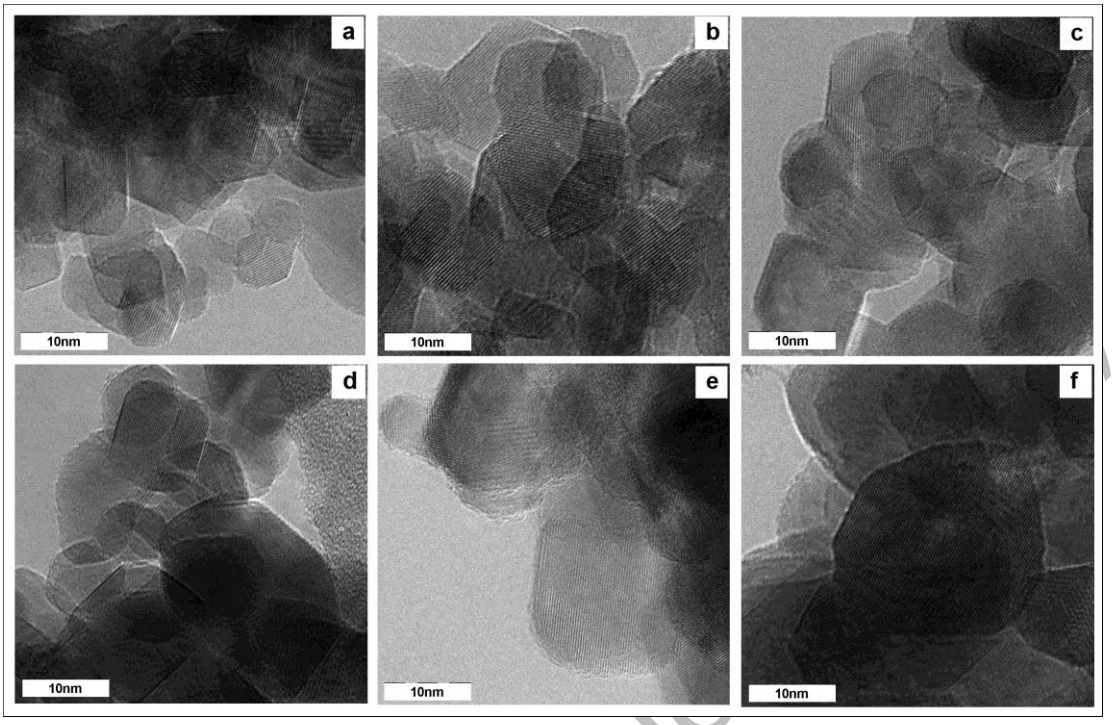

Figure 4. HRTEM micrographs of (a) TiO_2, (b) Cu, (c) 10Cu1Fe, (d) 9Cu2Fe, (e) 8Cu3Fe and (f) Fe

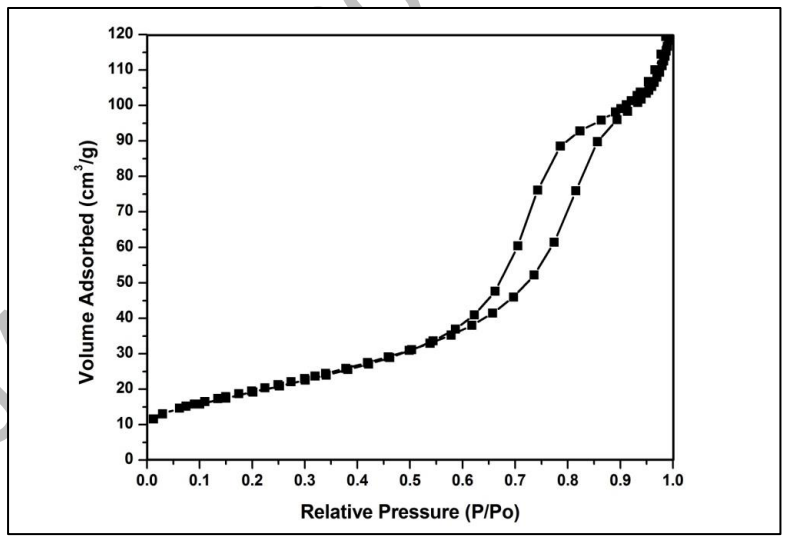

Figure 5. N_2 adsorption-desorption isotherm of 10Cu1Fe

Fourier Transform Infrared

Figure 6 exhibits the FTIR transmission spectra of Cu-Fe/TiO_2 with different Cu:Fe mass composition with additional 7Cu4Fe. For all the spectra, the broad band around 3400 cm^{-1} was attributed to O-H stretching, and the peak near 1600 cm^{-1} to H-O-H bending [38]. These peaks might be due to the physically adsorbed water. The broad band observed between 400 – 900 cm^{-1} corresponds to the Ti-O stretching vibrations [39]. FTIR is not a suitable

technique to detect the presence of Cu, Fe or Cu-Fe species since the metal–O vibrations are not IR-active. However, these species were detected using EDX.

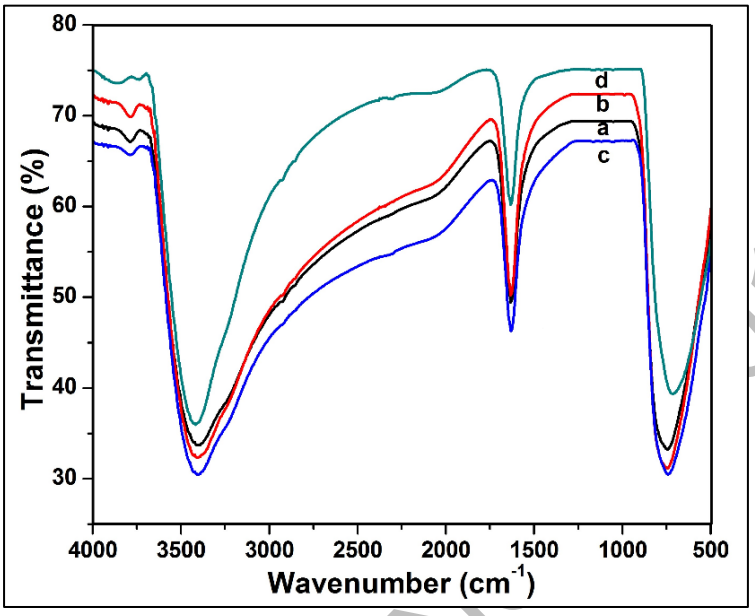

Figure 6. FTIR spectra of (a) 10Cu1Fe, (b) 9Cu2Fe, (c) 8Cu3Fe and (d) 7Cu4Fe

Diffuse Reflectance UV-Visible Spectroscopy

The DR-UV-Vis spectra of the photocatalysts are depicted in Figure 7. The absorption spectrum for TiO_2 shows an absorption edge at 400 nm corresponding to the band gap of 3.09 eV. The absorption band at 323 nm is generally related to the electronic excitation from the valence band O 2p electron to conduction band Ti 3d orbital indicating that Ti is in the form of tetrahedral Ti^{4+} species [40]. All Cu-Fe co-doped photocatalyst shows considerable shift of the absorption edge towards visible region compared to TiO_2. In general, as the Fe content increases, the absorption in the visible region (400 – 780 nm) also increases. It has been generally accepted that the metal dopants introduces a new energy level into the band gap of TiO_2 which is close and above the valence band. Thus, the charge transfer from the valence band to the conduction band from the new energy level requires lower photon energy at lower wavelength [41]. TiO_2 sample doped with Cu-Fe doped TiO_2 sample showed substantial and broader absorption shoulder up to 800 nm. The extended absorption of metal doped TiO_2 samples into the visible region has been explained in terms of excitation of electrons of dopant ion to TiO_2 conduction band. For example, the enhanced absorption observed for the metal doped TiO_2 samples doped with Fe, Cu and Cu-Fe in visible region can be considered to involve excitation of 3d electrons of dopant ion to TiO_2 conduction band according to their respective energy levels [42]. The enhancement of light absorption in the visible region provides a possibility for improving the photocatalytic performance of TiO_2 under visible light irradiation. Doping with Cu-Fe could create sub band states in the band gap of TiO_2 which can then be easily excited to produce more electron-hole pairs under visible light irradiation, hence resulting in higher photocatalytic performance compared to undoped TiO_2. Moreover, a decrease in the band gap energy together with an enhanced absorption intensity of all doped TiO_2 can be seen from the UV-Vis results. This pheonomenon could be due to many factors such as morphology, crystallite size, phase structure and amount of metal loadings [43].

In order to determine the band gap energy of the photocatalyst, reflectance [F(R)] spectra using Kubelka-Munk formalism and Tauc plot was employed for each synthesized photocatalyst [44]. Using the Tauc plot of $[F(R).hv]^n$ vs. hv where hv is the photon energy and n = ½ for direct band gap of the photocatalyst, the linear region of the plot

was extrapolated to intersect the photon energy axis to deduce the band gap energy of the respective photocatalyst. The band gap of bare TiO_2 was 3.09 eV and upon incorporation of Cu, Fe or Cu-Fe, the band gap values were reduced. The band gap for Cu was 2.70 eV. The incorporation of Cu and Fe at 10:1 mass composition gave the highest reduction to the band gap (2.69 eV). As the Fe content increases, the band gaps slowly increases from 2.72 to 2.73 eV for 9Cu2Fe and 8Cu3Fe, respectively, indicating some synergistic effect [43]. The band gap for Fe was the highest, 2.82 eV. The blue shift in the absorption of photocatalysts suggested that the dopants successfully generate lower energy level between the valence and conduction bands [45]. The estimated band gap energy of metal doped TiO_2 was lower compared to that of TiO_2 P25 (3.2 eV) [46]. Decreasing band gap energy increases the absorbance in the visible region and indicates that the electron-hole pairs can be generated with metal doping on the TiO_2, which can be attributed to the charge transfer between metal ions and TiO_2 [34].

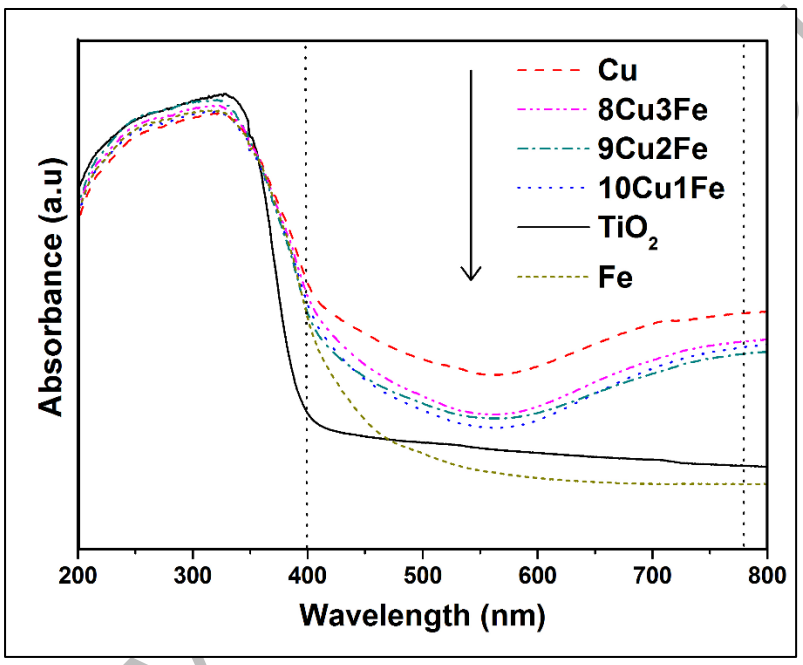

Figure 7. DR-UV-Vis spectra of TiO_2, Cu, 10Cu1Fe, 9Cu2Fe, 8Cu3Fe and Fe

Photocatalytic performance

The mass composition of metals in the bimetallic photocatalyst plays a significant role in the photocatalytic activity [47]. Figure 8 displays the photooxidative efficiency for DBT conversion of model diesel using the photocatalysts with different Cu:Fe mass composition. The highest DBT conversion was 82.36 % displayed by 10Cu1Fe. It is noteworthy that the monometallic photocatalysts displayed the lowest DBT conversion of 18.95 % for Fe and 54.88 % for Cu compared to the bimetallic photocatalysts. This observation is similar to studies reported by Liu et al. [24] and Zhang [25], where the photocatalytic activity of Cu-Fe co-doped TiO_2 was higher than that of undoped or singly doped photocatalyst.

The formation of electron-hole pairs ($e_{cb}^- - h_{vb}^+$) are important in the photooxidation of DBT. During photooxidation process, the electrons (e_{cb}^-) in the valence band were excited by photons from the light energy. Excited electrons migrate to the conduction band leaving holes in the valence band. Both the electrons (e_{cb}^-) and the holes (h_{vb}^+) can react with entities in the system to produce hydroxyl radicals (•OH) with an oxidation potential of 2.8 V. By incorporating Cu and Fe metals, the recombination rate of $e_{cb}^- - h_{vb}^+$ pairs can be reduced by trapping these charges. The electrons can be trapped by Cu^{2+} ions to form Cu^+ or CuO. The potential of Cu^{2+}/Cu^+ (0.17 V) and Cu^+/CuO (0.52 V) are thermodynamically feasible since an electron trapper could provide better separation

between the electrons and holes compared to TiO_2 (−0.2 V) alone. Because of this, more holes are available for the photooxidation process. On the other hand, Fe^{3+} can become a trapper for both the electrons and holes simultaneously forming Fe^{2+} and Fe^{4+}, respectively. This is possible due to the energy levels of Fe^{3+}/Fe^{4+} and Fe^{2+}/Fe^{3+} that lie above the valence band and below the conduction band of TiO_2. Theoretically, the stability of Fe^{2+} and Fe^{4+} are lower compared to Fe^{3+} which has a half-filled $3d^5$ orbital configuration. Hence, Fe^{2+} can easily release the trapped electron to be oxidized back to Fe^{3+} which then migrates to the surface to initiate photocatalytic reaction. Fe^{4+} can be reduced to Fe^{3+} by donating the trapped holes to combine with the surface OH groups to give •OH. When the Cu:Fe mass composition were 9:2 and 8:3, the DBT conversion were 74.58 and 75.24 %, respectively.

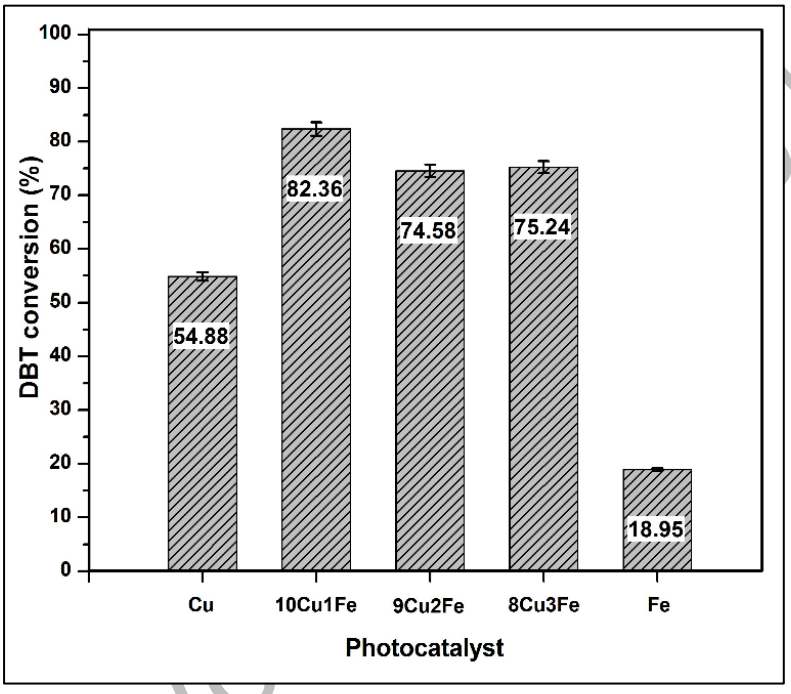

Figure 8. DBT conversion using Cu, 10Cu1Fe, 9Cu2Fe, 8Cu3Fe and Fe

Conclusion

The incorporation of Cu-Fe onto TiO_2 nanoparticles was able to reduce the band gap from 3.09 to as low as 2.69 eV for photocatalyst with Cu:Fe 10:1 mass composition. The lowering of band gap is an indication of shifting of the absorption edge to visible light region, which is important for photocatalysts to harvest energy from the free and abundant sunlight. The presence of bimetallic Cu-Fe co-catalyst was able to enhance the photoactivity of TiO_2 under visible light illumination. Photodegradation of 100 ppm DBT in model diesel using 10Cu1Fe in the presence of H_2O_2 has led to 82.36 % DBT conversion. Although the photocatalyst displayed good DBT degradation, the oxidized sulfur species which are retained in the model oil need to be removed. An integrated photodegradation-extraction system is required to photooxidize the sulfur species followed by removal of the oxidized compounds.

Acknowledgement

The authors extend their utmost gratitude for the financial support and research facilities provided by Yayasan UTP, MyPhD and FRGS from the Ministry of Education, Malaysia; and the Centre of Research in Ionic Liquid (CORIL), Universiti Teknologi PETRONAS.

References

1. Srivastava, V. C. (2012). An evaluation of desulfurization technologies for sulfur removal from liquid fuels. *RSC Advances*, 2: 759 – 783.
2. Zhang, J., Zhao, D. S. and Wang, J. L. (2009). Photocatalytic oxidation of dibenzothiophene using TiO_2/bamboo charcoal. *Journal of Materials Science*, 44: 3112 – 3117.
3. Maricq, M. M., Chase, R. E., Xu, N. and Laing, P. M. (2002). The effects of the catalytic converter and fuel sulfur level on motor vehicle particulate matter emissions: Light duty diesel vehicles. *Environmental Science & Technology*, 36: 283 – 289.
4. Campos-Martin, J. M., Capel-Sanchez, M. C., Perez-Presas, P. and Fierro, J. L. G. (2010). Oxidative processes of desulfurization of liquid fuels. *Journal of Chemical Technology and Biotechnology*, 85: 879 – 890.
5. Jiang, Z., Lu, H., Zhang, Y. and Li, C. (2011). Oxidative desulfurization of fuel oils. *Chinese Journal of Catalysis*, 32(5): 707 – 715.
6. Lina, Y., Jian, L., Xingdong, Y., Shen, J. and Yutai, Q. (2007). One step non-hydrodesulfurization of fuel oil: catalyzed oxidation adsorption desulfurization over HPWA-SBA-15. *Journal of Molecular Catalysis A: Chemical*, 262: 114 – 118.
7. Lu, H., Deng, C., Ren, W. and Yang, X. (2014). Oxidative desulfurization of model diesel using $[(C_4H_9)_4N]_6Mo_7O_{24}$ as a catalyst in ionic liquids. *Fuel Process Technology*, 119: 87 – 91.
8. Ban, L. L., Liu, P., Ma, C. H. and Dai, B. (2013). Deep extractive desulfurization of diesel fuel by $FeCl_3$/ionic liquids. *Chinese Chemistry Letters*, 24:755 – 758.
9. Rodriguez-Cabo, B., Rodriguez, H., Rodil, E., Arce, A. and Soto, A. (2014). Extractive and oxidative–extractive desulfurization of fuel with ionic liquids. *Fuel*, 117: 882 – 889.
10. Li, W. L., Tang, H., Liu, Q., Xing, J., Li, Q., Wang, D., Yang, M., Li, X. and Liu, H. (2009). Deep desulfurization of diesel by integrating adsorption and microbial method. *Biochemical Engineering Journal*, 44: 297 – 301.
11. Kim, H., Ma, X., Zhou, A. and Song, C. (2006). Ultra-deep desulfurization and denitrogenation of diesel fuel by selective adsorption over three different adsorbents: a study on adsorptive selectivity and mechanism. *Catalysis Today*, 111:74 – 83.
12. Dinamarca, M. A., Ibacache-Quiroga, C., Baeza, P., Galvez, S., Villarroel, M., Olivero, P. and Ojeda, J. (2010). Biodesulfurization of gas oil using inorganic supports biomodified with metabolically active cells immobilized by adsorption. *Bioresource Technology*, 101: 2375 – 2378.
13. Fatemeh, D. D., Manouchehr, V. and Abed, A. Z. (2010). Biodesulfurization of dibenzothiophene by newly isolated rhodococcus erythropolis strain. *Bioresource Technology*, 101:1102 – 1105.
14. Hirai, T., Ogawa, K. and Komasawa, I. (1996). Desulfurization process for dibenzothiophenes from light oil by photochemical reaction and liquid-liquid extraction. *Industrial and Engineering Chemical Research*, 35: 586 – 589.
15. Shiraishi, Y., Hirai, T. and Komasawa, I. (2002). TiO_2-mediated photocatalytic desulfurization process for light oils using an organic two-phase system. *Journal of Chemical Engineering of Japan*, 35: 489 – 492.
16. Huang, Y., Ho, W., Ai, Z., Song, X., Zhang, L. and Lee, S. (2009). Aerosol-assisted flow synthesis of B-doped, Ni doped and B–Ni-codoped TiO_2 solid and hollow microspheres for photocatalytic removal of NO. *Applied Catalysis B*, 89:398 – 405.
17. Liu, G. Q., Jin, Z. G., Liu, X. X., Wang, T. and Liu, Z. F. (2006). Anatase TiO_2 porous thin films prepared by sol-gel method using CTAB surfactant. *Journal of Sol-Gel Science and Technology*, 41: 49 – 55.
18. Ibrahim, A., Xian, S. B. and Wei, Z. (2003). Desulfurization of FCC gasoline by solvent extraction and photooxidation. *Petroleum Science and Technology*, 21: 1555 – 1573.
19. Zhao, D., Li, F., Han, J. and Li, H. (2007). Photochemical oxidation of thiophene by O_2 in an organic two-phase liquid-liquid extraction system. *Petroleum Chemistry*, 47: 448 – 451.
20. Shiraishi, Y., Hirai, T. and Komasawa, I. (1999). Identification of desulfurization products in the photochemical desulfurization process for benzothiophene and dibenzothiophene from light oil using an organic two-phase extraction system. *Industrial and Engineering Chemical Research*, 38: 3300 –3309.
21. Song, C. (2003). An overview of new approaches to deep desulfurization for ultra-clean gasoline, diesel and jet fuel. *Catalysis Today*, 86: 211 – 263.

22. Matsuzawa, S., Tanaka, J., Sato, S. and Ibusuki, T. (2002). Photocatalytic oxidation of dibenzothiophene in acetonitrile using TiO_2: effect of hydrogen peroxide and ultrasound irradiation. *Journal of Photochemistry and Photobiology A*, 149: 183 – 189.
23. Shiraishi, Y., Hirai, T. and Komasawa, I. (2001). Photochemical desulfurization and denitrogenation process for vacuum gas oil using an organic two-phase extraction system. *Industrial and Engineering Chemical Research*, 40: 293 – 303.
24. Liu, J, Zhang, Z, Yang, L, Zhang, Y, Deng S. (2011). The degradation of reactive black wastewater by Fe/Cu co-doped TiO_2. *International Journal of Chemistry*, 3: 87 – 92.
25. Zhang, D. (2010). Enhanced photocatalytic activity for titanium dioxide by commodification with copper and iron. *Transition Metal Chemistry*, 35: 933 – 938.
26. Zaid, H. F. M., Chong, F. K. and Mutalib, M. I. A. (2014). Integrated photooxidative–extractive desulfurization system for fuel oil using Cu, Fe and Cu–Fe/TiO_2 and eutectic based ionic liquids: effect of calcination temperature and duration. *AIP Conference Proceedings*, 1621: 231 – 237.
27. Khan, M. A., Akhtar, M. S. and Yang, O. B. (2010). Synthesis, characterization and application of sol–gel derived mesoporous TiO_2 nanoparticles for dye-sensitized solar cells. *Sol Energy*, 84: 2195 – 2201.
28. Vijayalakshmi, R. and Rajendran, V. (2012). Synthesis and characterization of nano-TiO_2 via different methods. *Archives Applied Science Research*, 4:1183 – 1190.
29. Kim, D. S. and Kwak, S. Y. (2007). The hydrothermal synthesis of mesoporous TiO_2 with high crystallinity, thermal stability, large surface area, and enhanced photocatalytic activity. *Applied Catalysis A: General*, 323: 110 – 118.
30. Yu, J., Zhao, X. and Zhao, Q. (2000). Effect of surface structure on photocatalytic activity of TiO_2 thin films prepared by sol–gel method. *Thin Solid Films*, 379: 7 – 14.
31. Wu, Y., Zhang, J., Xiao, L. and Chen, F. (2009). Preparation and characterization of TiO_2 photocatalysts by Fe^{3+} doping together with Au deposition for the degradation of organic pollutants. *Applied Catalysis B: Environment*, 88: 525 – 532.
32. Yoong, L. S., Chong, F. K. and Dutta, B. K. (2009). Development of copper-doped TiO_2 photocatalyst for hydrogen production under visible light. *Energy*, 34: 1652 – 1661.
33. Kim, A. Y. and Kang, M. (2012). Effect of Al-Cu bimetallic components in a TiO_2 framework for high hydrogen production on methanol/water photo-splitting. *International Journal of Photoenergy*, 2012:1-9.
34. Nurlaela, E., Chong, F. K., Dutta, B. K. and Riaz N. (2010). Bimetallic Cu–Ni/TiO_2 as photocatalyst for hydrogen production from water. *International Conference on Fundamental and Applied Sciences (ICFAS2010).* Kuala Lumpur, Convention Center, KL.
35. Zhu, J., Chen, F., Zhang, J., Chen, H. and Anpo, M. (2006). Fe^{3+}–TiO_2 photocatalysts prepared by combining sol–gel method with hydrothermal treatment and their characterization. *Journal of Photochemistry and Photobiology A: Chemistry*, 180: 196 – 204.
36. Lu, C. H., Wu, W. H. and Kale, R. B. (2008). Microemulsion-mediated hydrothermal synthesis of photocatalytic TiO_2 powders. *Journal of Hazardous Materials*, 154: 649 – 654
37. Aeroxide and Aeroperl. (2005). Technical information (1243) for Aeroxide and Aeroperl titanium Dioxide as photocatalyst; Bulletin No. 1-1243-0:1-14.
38. Li, D., Haneda, H., Hishita, S. and Ohashi, N. (2005). Visible-light driven nitrogen-doped TiO_2 photocatalysis: Effect of nitrogen precursors on their photocatalysis for decomposition of gas-phase organic pollutants. *Materials Science and Engineering B*, 52: 843 – 850.
39. Yan, X., He, J., Evans, D. G., Zhu, Y. and Duan, X. (2004). Preparation, characterization and photocatalytic activity of TiO_2 formed from mesoporous precursor. *Journal of Porous Materials*, 11:131 – 139.
40. Fuerte, A., Hernandez-Alonso, M. D., Maira, A. J., Martinez-Arias, A., Fernandez-Garcia, M., Conesa, J. C., Soria, J. and Munuera, G. (2002). Nanosize Ti-W mixes oxides: Effect of doping level in the photocatalytic degradation of toluene using sunlight type excitation. *Journal of Catalysis*, 212: 1 – 9.
41. Cao, H., Lin, X., Zhan, H., Zhang, H. and Lin J. (2013). Photocatalytic degradation kinetics and mechanism of phenobarbital in TiO_2 aqueous solution. *Chemosphere*, 90: 1514 – 1519.
42. Nahar, M. S., Hasegawa, K. and Kagaya, S. (2006). Photocatalytic degradation of phenol by visible light-responsive iron-doped TiO_2 and spontaneous sedimentation of the TiO_2 particles. *Chemosphere*, 65: 1976 – 1982.

43. Li, H., Zhang, Y., Wang, S., Wu, Q. and Liu, C. (2009). Study on nanomagnets supported TiO_2 photocatalysts prepared by a sol–gel process in reverse microemulsion combining with solvent-thermal technique. *Journal of Hazardous Materials*, 169: 1045 – 1053.
44. Murphy, A. B. (2007). Band-gap determination from diffuse reflectance measurements of semiconductor films, and application to photoelectrochemical watersplitting. *Solar Energy Materials Solar Cells*, 91: 1326 – 1337.
45. Wu, D., Long, M., Cai, W., Chen, C. and Wu, Y. (2010). Low temperature hydrothermal synthesis of N-doped TiO_2 photocatalyst with high visible-light activity. *Journal of Alloys and Compounds*, 502: 289 – 294.
46. Yalçin, Y., Kiliç, M. and Çinar, Z. (2010). Fe^{+3}-doped TiO_2: a combined experimental and computational approach to the evaluation of visible light activity. *Applied Catalysis B: Environment*, 99: 469 – 477.
47. Singto, S., Sorapong, P., Yoshikazu, S. and Susumu, Y. (2005). Photocatalytic activity of titania nanocrystals prepared by surfactant-assisted templating method – Effect of calcination conditions. *Materials Letters*, 59: 2965 – 2968.